Point-projection imaging of macromolecular contours

by J. A. PANITZ, *Sandia National Laboratories, Surface Physics Division* 5114, *Albuquerque, New Mexico* 87185, *U.S.A.*

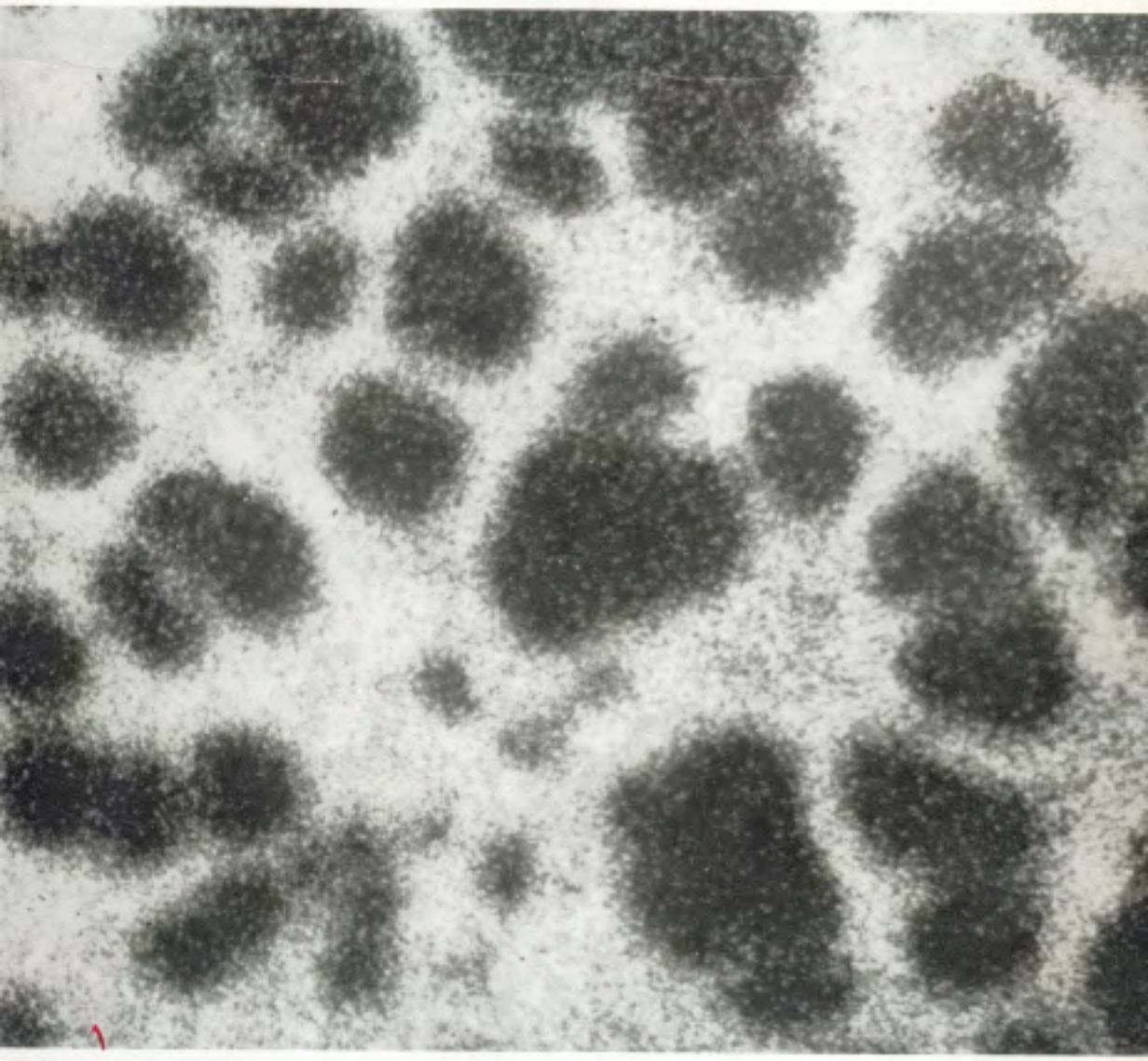

Reprinted from

Journal of Microscopy

Volume 125, Part 1, January 1982

Journal of Microscopy, *Vol.* 125, *Pt* 1, *January* 1982, *pp.* 3–23.
Revised paper accepted 20 *July* 1981

Point-projection imaging of macromolecular contours

by J. A. PANITZ, *Sandia National Laboratories**, *Surface Physics Division* 5114, *Albuquerque*, *New Mexico* 87185, *U.S.A.*

SUMMARY

A point-projection microscope is described which uses an electric field of several volts per nanometre to generate ions from a layer of benzene condensed in high vacuum on to the apex of a cryogenically cooled field-emitter tip. Clusters of ferritin (a spherical protein molecule) embedded in the layer, have been imaged by exposing their contours during controlled field-desorption. Image contrast is high. A magnification of 2×10^5 has been achieved at a spatial resolution estimated to be better than 3 nm. Three-dimensional reconstructions of cluster morphology from a series of molecular contours are in qualitative agreement with transmission-electron micrographs of the ferritin covered emitter apex. Reproducibility of the cluster contours, and TEM images of the apex before and after imaging suggest that the imaging procedure is nondestructive.

INTRODUCTION

For the past 30 years, attempts have been made to use the field-electron emission microscope (FEEM) and the field-ion microscope (FIM) to image organic molecules (Müller, 1950a, b, 1953a; Melmed, 1958; Melmed & Müller, 1958; Gurney *et al.*, 1965; Müller & Rendulic, 1967; Graham *et al.*, 1973). These attempts were inspired by the simplicity of the techniques and the potential for achieving high image contrast, magnification and resolution. By 1950 the FEEM had demonstrated a usable magnification of 10^6, and an image resolution better than 2 nm. As a result there was growing optimism that individual molecules might eventually be imaged. However, the field-electron emission pattern is very sensitive to surface contamination (Müller, 1953a), so that one could only hope to use the FEEM to examine molecules which could be vapour deposited on to a clean field-emitter tip in ultra high vacuum. Although striking images displaying the correct symmetry of flaventrene and copper-phthalocyanine were observed (Müller, 1950c, 1952), it soon became apparent that identical FEEM patterns were produced by a wide range of different molecular structures (Wolf, 1954). It appeared that the FEEM patterns were displaying some feature common to each deposited species but not the shape of any given molecule (Müller, 1953b; Hörl & Strangler, 1956; Komar & Komar, 1961).

The low temperature FIM (Müller, 1956a, b) provided another opportunity for examining molecular structure, but with greatly improved image resolution (0·2 nm under optimum conditions). Although macromolecules of biological interest could, in principle, be deposited on to the specimen surface from aqueous solution (Abbott, 1965), the high field strength required for field-ion imaging proved to be a major obstacle. Whereas electron-emission fields of 2–5 V/nm did not appear to damage an adsorbed molecule, the higher field strengths required for conventional field-ionization could destroy or remove a molecule from the surface before imaging

* A U.S. Department of Energy facility.

was achieved (Becker & Brandes, 1956). The problem is probably associated with the electrostatic field stress associated with a minimum ion-imaging field, $F \approx 20$ V/nm. If a molecule behaves as a conducting protrusion on the tip apex, it will experience an outward directed, electrostatic stress whose magnitude is just the energy density of the electrostatic field: $\epsilon_0 F^2/2 = 1{\cdot}8 \times 10^9$ newtons/m^2 = 128 tons/in^2.

In order to shield a molecule from the effects of the imaging field, ingenious schemes were developed for embedding deposited molecules within a metallic matrix (Gurney *et al.*, 1965; Müller & Rendulic, 1967; Graham *et al.*, 1973). Another strategy (Machlin, 1971; Machlin *et al.*, 1975) attempted to record transient ion images of deposited molecules at the earliest stages of image formation. Unfortunately, the resulting images were not particularly convincing. Most images did not reflect the known structure of the imaged species; many were transient, and few were reproducible.

In this paper we will present another approach to the problem of imaging biological molecules deposited on field-emitter tips. The procedure has evolved over several years (Panitz & Giaever, 1979, 1980a; Panitz, 1981) and seems to be capable of providing non-transient, reproducible images of at least one protein macromolecule, ferritin. Although ferritin is essentially spherical in shape, it is a unique molecule for our purposes in that it contains at its core some 5000 iron atoms. Since the core scatters electrons effectively, it can be observed in the transmission electron microscope (TEM). As a result, we have been able to determine, for the first time, the distribution of molecules on a field-emitter tip independent of the high-field images which are observed. Consequently, we have confidence that our images of ferritin actually represent a distribution of molecules on the apex of a field emitter tip. Furthermore, TEM micrographs taken before and after imaging strongly suggest that our imaging process is nondestructive.

EARLY IMAGING ATTEMPTS

Our first imaging attempts were conducted in 1976 without knowing if, and how, molecules were distributed on the tip surface. The images obtained were highly structured, but could not be reproduced. In this sense, the microscopy was similar to previous high-field attempts to image biomolecules. On the other hand, the images were nontransient, and were obtained at field strengths well below those required for hydrogen field-ion imaging of a metal surface (i.e. well below 20 V/nm).

Guided only by field-ion considerations and a desire to produce highly magnified images at high resolution, relatively sharp tips of tungsten were prepared by electrochemical polishing (Müller & Tsong, 1969). Those having a radius below 30 nm (as judged by the ability to obtain a helium ion image below 8 kV) were selected for further processing. This involved increasing the tip radius by controlled field-evaporation until a relatively perfect helium FIM image was obtained over a wide field-of-view (typically greater than 40° as measured from the tip axis). Helium best image voltages ranged from 10 to 20 kV, corresponding to tip radii between 40 and 90 nm.

Protein solutions were prepared by dilution in distilled water. Protein concentration was not directly determined, but was judged to be usable from a simple, visual test of protein adsorption (Giaever, 1973). Tips were dipped into the protein solution, apex first. After remaining immersed for a predetermined length of time they were withdrawn and rinsed by inserting (apex first) into distilled water in the hope of removing any poorly attached protein or protein residue. After rinsing, the tips were placed in a vacuum system which was ion-pumped to 2 μPa over a period of 12 h. At the end of the pumpdown period, a tip was cooled to $\sim$80 K with liquid nitrogen. It was clear from previous studies that conventional field-ion microscopy could not be used for imaging because of the high field strengths which were required. Another imaging strategy was needed.

During an unsuccessful attempt to image the position of carbon atoms in a benzene ring by field-desorption (Panitz, 1975), we discovered that a benzene molecule condensed on tungsten

below 90 K in a multilayer structure could be removed as a positive ion at a very low field strength. Furthermore, the images obtained by desorbing benzene from condensed multilayers at 80 K revealed a relatively high ionization efficiency, and uniform image contrast. These observations suggested that a biological molecule might be imaged by condensing benzene on to a field-emitter tip coated with biomolecules, and then field-desorbing the benzene from the surface of the adsorbed species. One might suspect that benzene would chemisorb strongly to the tungsten tip surface but be bound more weakly to the surface of the macromolecule of interest. This difference in binding could lead to a considerable difference in desorption field, allowing benzene to be preferentially removed from the molecule in order to image its morphology.

Benzene was admitted to the vacuum system at a pressure of 130 μPa. The coverage of benzene was determined by the rate of adsorption from the gas phase ($\sim$1 monolayer/second), and the rate of field-induced desorption. Field-desorption was initiated by a low DC tip bias (typically 0·5 kV), and a continuous train of superimposed, 50 ns wide pulses whose amplitude could be varied between 0·5 and 3 kV. First, the DC bias was adjusted until a faint, tenuous image was seen. At this point the tip was manipulated until the image was centred on the fluorescent screen of a chevron CEMA detector (Panitz, 1978). The DC bias was then reduced about 10% and the train of desorption pulses applied to the tip at a rate of $\sim$1 p.p.s. The pulse amplitude was increased until an image was observed. By varying the time between pulses, the brightness of the image could be varied, indicating that the image spot density was proportional to the pulse interval. This suggested that benzene was being adsorbed from the gas phase between successive desorption pulses. Since the benzene coverage at the start of an imaging sequence could not be determined, the equilibrium coverage of benzene during imaging could not be estimated.

It was tempting to assume that the coverage of benzene was slight. However, enough benzene could have condensed on to the tip apex prior to imaging to form a benzene crystal. If a benzene crystal had formed, structure in the image could be attributed to desorption of benzene from sharp crystal edges or facet boundaries. This was our major concern in evaluating the highly structured images which we observed.

Figure 1 shows an image of a 10 kV tip which had been dipped into human IgG, a Y-shaped immunoglobulin molecule. The image was stable for at least 0·5 h. After many minutes of imaging, the imaging voltages were decreased whereupon the image changed to that shown in Fig. 2. This image was stable for many minutes until a sudden bright flash appeared on the CEMA screen. After the flash, all structure disappeared, and only the image shown in Fig. 3 could be obtained. This image was characteristic of a 'clean' tip (i.e. a tip which had not been immersed in human IgG). Although several other tips were immersed into human IgG, the images shown in Figs. 1 and 2 could not be reproduced. However, another type of structured image was obtained, and is shown in Fig. 4. This image was stable until an increase in tip voltage caused a bright flash to appear on the CEMA screen. Then all structure in the image vanished.

The bright flash on the CEMA screen soon became the 'dreaded green flash' (the CEMA phosphor was green), which signalled the end of an imaging experiment. It was clear that something had changed on the tip surface after the green flash was observed. The flash resulted from a momentary saturation of the CEMA detector which was operated at a gain of at least 10^5. We could not tell if the bright flash corresponded to the dissociation and desorption of deposited molecules on the surface, or a thick, crystalline layer of condensed benzene.

Figure 5 shows the result of imaging a tip which had been dipped into bovine serum albumin (BSA), a small elliptically shaped molecule $\sim 3\,\text{nm} \times 6\,\text{nm}$ in size. To improve signal-to-noise, the CEMA detector was time-gated (Panitz, 1978) for the arrival of benzene. This required increasing the CEMA gain from zero to a maximum during a 20 ns wide time-window, 700 ns after the application of each desorption pulse. In order to define the coverage of benzene more exactly, a capillary doser was employed which could precisely control the amount of benzene deposited on the tip (Panitz, 1979a). Between each desorption pulse, the doser was extended so that benzene issuing from an orifice at its end could strike the tip apex directly. The doser was then retracted, preventing benzene from reaching the tip apex. Although the benzene exposure

could be exactly reproduced between each desorption pulse, the capillary was not calibrated so that the coverage of benzene was not known.

Figure 6 is an image of the same tip (under the same imaging conditions) taken earlier in the experiment. Such an image might be produced by a cluster of BSA molecules deposited on the surface. The later image shown in Fig. 5 could then be explained if we assume that most of the cluster had field-desorbed during imaging, leaving one or two BSA molecules on the surface. Figure 7 shows the result of imaging after the green flash. Several other tips were dipped into BSA but no structured images were obtained although a wide range of benzene deposition parameters were tried.

Since the controlled dosing procedure made the formation of a benzene crystal unlikely, our inability to reproduce structured images suggested that there might be a problem with placing molecules on the tip surface. It was not clear if the method of depositing molecules was at fault,

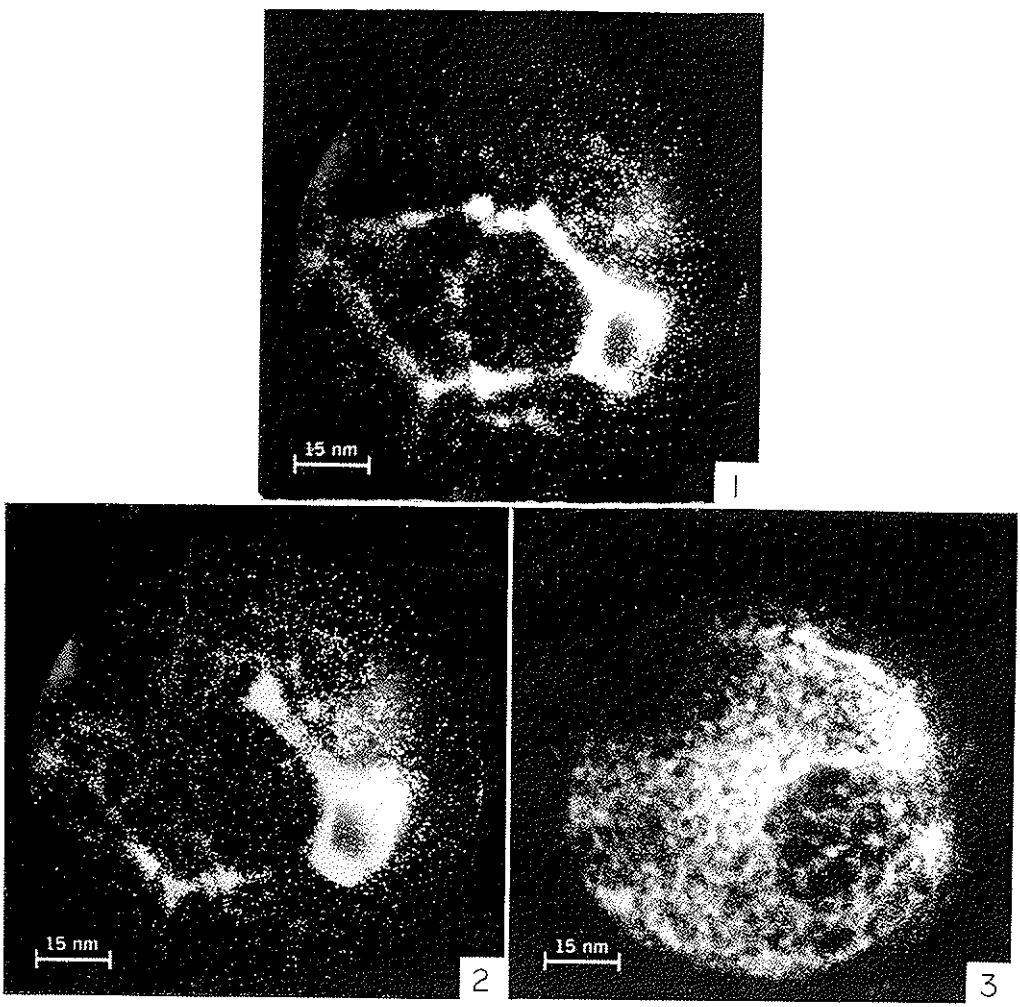

Fig. 1. An early image obtained from a 10 kV (helium BIV) tungsten field emitter dipped in human IgG and imaged at 80 K by pulsed benzene desorption. Background pressure = 130 μPa C_6H_6. Sum of 100 pulses 0·8 s apart. Pulse amplitude ~1 kV. Tip bias = 1·73 kV.

Fig. 2. Same imaging conditions as Fig. 1, but pulse amplitude ~1·7 kV; tip bias = 0·5 kV.

Fig. 3. Same imaging conditions as Fig. 2, after a bright 'flash' was observed on the CEMA screen. The pattern is characteristic of pulsed benzene desorption from a clean tip at 80 K.

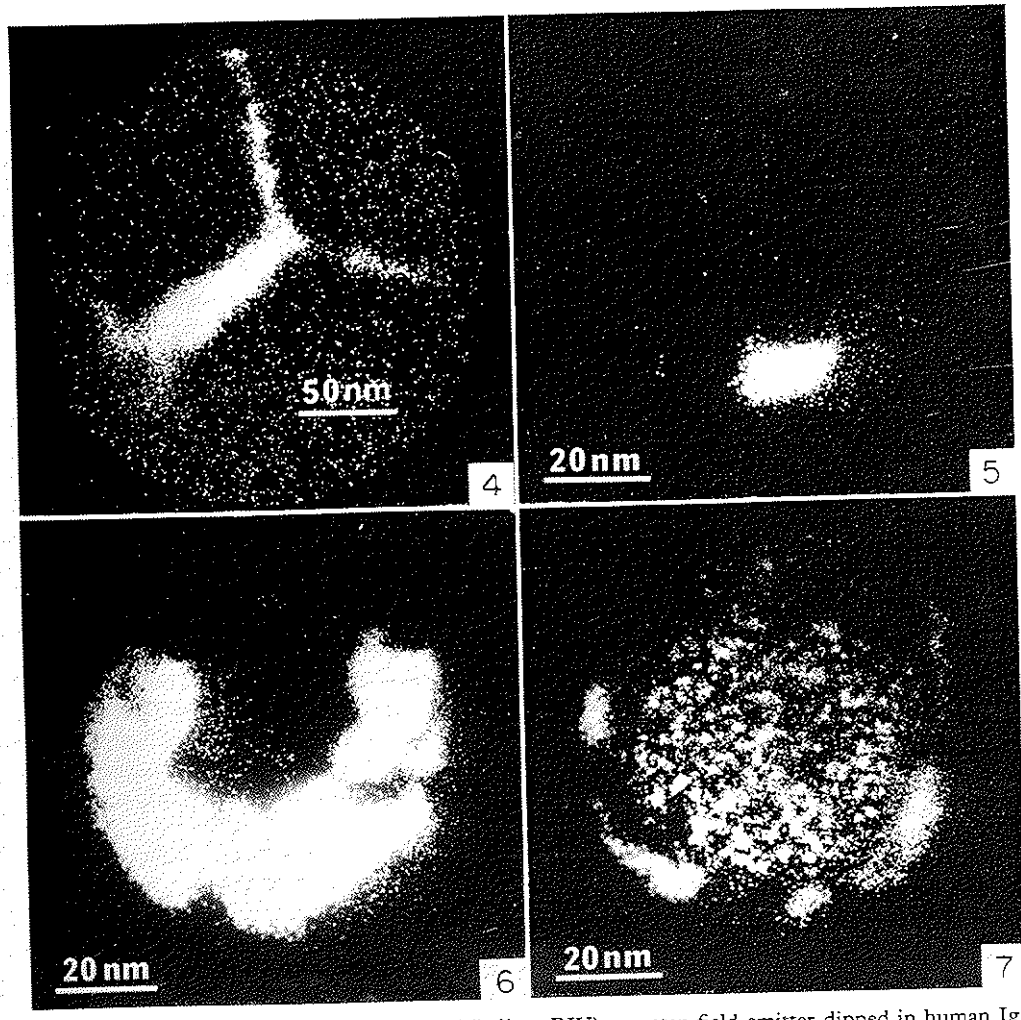

Fig. 4. An early image obtained from a 10 kV (helium BIV) tungsten field emitter dipped in human IgG and imaged at 90 K by pulsed benzene desorption. Sum over several desorption pulses. Pulse amplitude ~1·0 kV. Tip bias = 0·8 kV.

Fig. 5. An early image obtained from a 10 kV (helium BIV) tungsten field-emitter dipped in bovine serum albumin (BSA) and imaged at 90 K by pulsed benzene desorption. Benzene coverage was controlled by a retractable capillary doser. During pulsing, background pressure = 000 μPa. Sum of > 200 pulses 91·5 s apart. Pulse amplitude ~1·2 kV. Tip bias = 0. The CEMA detector was time gated for the arrival of $C_6H_6^+$ (700 ns delay time). Image suggests clustering of a few BSA molecules. The micron marker shown in this figure should only be used as a qualitative indication of feature size. A precise calibration of image magnification is not available.

Fig. 6. Same tip and imaging conditions as in Fig. 5, but a sum over 138 pulses, 1·5 s apart. The image (recorded before the image of Fig. 5) suggests that a large cluster of BSA molecules was originally deposited on the surface. The micron marker shown in this figure should only be used as a qualitative indication of feature size. A precise calibration of image magnification is not available.

Fig. 7. Same imaging conditions as Fig. 6, after a bright flash was observed on the CEMA screen. The micron marker shown in this figure should only be used as a qualitative indication of feature size. A precise calibration of image magnification is not available.

or if the size of the image area was the limiting constraint. Since reasonably sharp tips were used, we could only view a surface area of perhaps 3000 nm^2. Unlike electron microscopy, we cannot choose an area for imaging from a much larger field-of-view. The deposition of molecules from aqueous solution is statistical in nature. This means that at the low protein concentrations required to obtain isolated molecules on the surface, the probability of obtaining a molecule within the imaged area of the tip could be quite small.

It appeared that our microscopy suffered from two serious problems: (1) an inability to reproducibly place low coverages of molecules on the viewable area of the tip apex, and (2) image interpretation. Even if a single molecule could be placed on the tip apex with assurance, it was not clear what portion of the molecule would be imaged. Would we see only the most protruding portion of the molecule's contour where the electric field might be the highest, or would we see only those regions where benzene would be most weakly bound?

SPECIMEN PREPARATION

In order to determine the feasibility of reproducibly placing a submonolayer coverage of molecules on the tip apex, we decided to re-evaluate the deposition procedures which had been previously reported in the FIM literature (Abbott, 1965; Graham *et al.*, 1973). In the past, the success of a deposition procedure was judged by the quality of the FEEM or FIM image which it produced. Since these images were never particularly convincing, the deposition procedures could not be realistically evaluated. In order to separate any difficulty with the imaging procedure from any problem associated with protein deposition, it is important to use an independent method to evaluate the success of the deposition. During a series of Imaging Atom-Probe experiments (Kellogg & Panitz, 1979), we had used the transmission electron microscope (TEM) to image the morphology of carbon layers deposited on to tungsten field-emitter tips in an operating Tokamak reactor. The results suggested that the TEM could also be used to image the morphology of unstained protein layers provided they were thick enough to be visible. The change in the morphology of these layers with a change in a deposition parameter might help to evaluate the importance of that parameter in the deposition procedure.

Studies of thick protein layers formed on field emitter tips by the antigen–antibody reaction (Panitz & Gieaver, 1980b) seemed to demonstrate that surface tension forces could alter the distribution of protein on the tip apex. In addition, electrochemical reactions between different metals involved in mounting a tip rigidly to a holder were shown to change the characteristics of the deposited layer. From these studies, three 'rules' for protein deposition were extracted: (1) ensure that the tip has as large an apex radius as possible; (2) ensure that the tip crosses a minimum number of liquid/air interfaces; and (3) ensure that only one metal is immersed in an aqueous protein solution at one time. Our experiments suggested that the sharp tips used in our early imaging attempts (and the method used for deposition) may have hindered reliable protein deposition.

In order to prepare a suitable, large radius tip, a tungsten rod was electropolished, and thermally annealed in high vacuum near its melting point. After annealing, a linear Fowler-Nordheim characteristic was determined. From its slope and intercept, and an independent (TEM) estimate of the tip radius, the conversion factor K between a potential applied to the tip and the resulting electric field strength was obtained. An iterative procedure was used to obtain K in which a value for the average work function of clean tungsten (4·5 eV) had to be assumed (Gomer, 1961).

The aqueous deposition procedure which evolved from the antigen–antibody studies was subsequently applied to ferritin, a nearly spherical protein molecule about 11 nm in diameter with a molecular weight of $\sim$460,000 Daltons. Since ferritin contains about 5000 iron atoms at its core it is electron-opaque, and its distribution can be directly observed on the surface of a field-emitter tip viewed in profile in the TEM. We quickly observed that a monolayer of ferritin could be easily and reproducibly achieved, but that submonolayer coverages were hardly ever obtained. The problem was eventually associated with the Blodgett-Langmuir effect. In 1931 Katharine Blodgett (and Irving Langmuir) observed that a monomolecular film of calcium stearate could

be deposited on a glass slide by passing the slide through a monolayer of stearic acid floating on water (Blodgett, 1935). In the present study, dipping a tip into a solution of ferritin resulted in a monolayer coverage because the abundance of ferritin at the air–liquid interface of the dosing solution is relatively independent of its concentration in solution. The trick is to avoid passing the tip through an interface where ferritin molecules can be found. The simple solution, shown schematically in Fig. 8, is to first immerse the tip into a diluent (in this case 0·154 N saline), and then add a ferritin solution. Several rinses without breaking the interface ensures that when the tip is finally withdrawn into air, no molecules will be available for further deposition. The results were successful (Panitz & Giaever, 1981) and implied that all previous FIM deposition procedures (including our own) were not particularly reliable.

IMAGE FORMATION

Although desorbing benzene from the surface of an adsorbed molecule seemed to be a reasonable imaging procedure, we were concerned because we could not tell which portion of the molecule was being imaged. In order to eliminate the resulting ambiguity when interpreting an image, an alternate imaging scheme was devised. It is essentially a shadowing technique. However, unlike a shadowing procedure in the TEM, we remove the shadowing species in order to form an image. Figure 9 shows the procedure in schematic form. A macromolecule of characteristic dimension, S_0, is deposited on to a field-emitter tip of apex radius, R, by deposition from aqueous solution. Since S_0 is generally much greater than any local surface feature, but much smaller than the apex radius of the tip, the molecule tends to act like a minor dielectric protrusion on an infinite metal plane. After placing the tip in ultra-high vacuum and cooling it below 30 K, a precise quantity of benzene is condensed on to the tip apex from the gas phase. The benzene covers or 'blankets' the surface, completely surrounding and covering the molecule in an immobile layer. Suppose that a potential V_0 is applied to the tip with respect to a sensitive ion detector at ground potential placed a distance, D, in front of the tip apex. If the condensed benzene

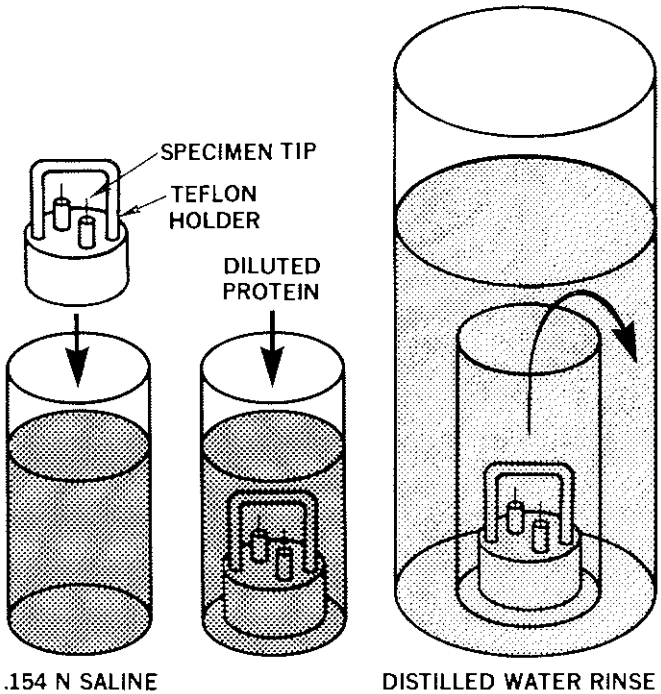

Fig. 8. A schematic drawing of the deposition procedure used to place submonolayer coverages of ferritin on large radius, field-emitter tips.

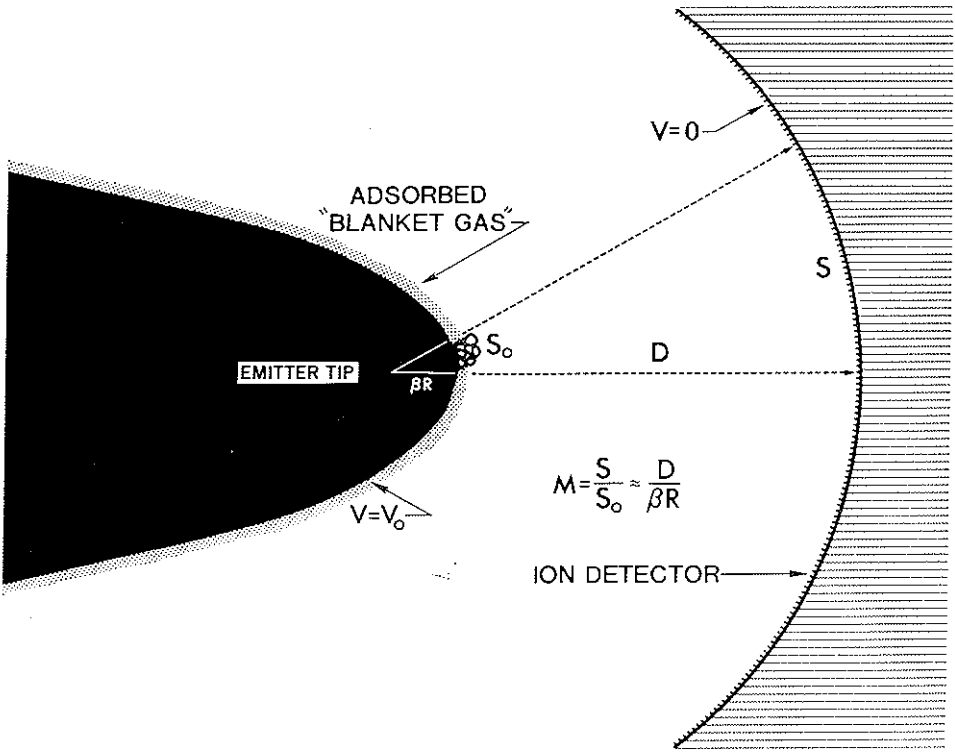

Fig. 9. A schematic drawing of a later stage in the point-projection imaging procedure used to obtain molecular images. The procedure begins by condensing a suitable 'blanket-gas' species on to the tip apex completely surrounding and covering a molecule (in this case ferritin) in an immobile layer. An electric field is then used to gradually desorb the blanket gas as positive ions, exposing the contour of the embedded ferritin at a well-defined elevation above the surface. A highly magnified image of the uncovering process appears in real time at a suitable ion detector.

layer is uniform, the resulting electric field at the benzene–vacuum interface will retain the symmetry determined by the spherical contour of the clean metal surface. Now imagine that the benzene in the outermost layer is ionized. The resulting ions will be projected to the detector where they will record a highly magnified image of their relative positions in the layer prior to the ionization event. Provided the ionization probability is high and relatively isotropic, the image will appear bright, and relatively contrastless.

If the rate of benzene desorption can be carefully controlled, the condensed multilayer can be gradually dissected. As long as a layer of benzene covers the adsorbed macromolecules, the detector image will appear relatively uniform. However, as soon as a molecule is exposed, a dark region will appear in the image. If the dielectric constant of the molecule is not greatly different from that of benzene, the electric field in the vicinity of the molecule will be essentially undistorted, and the contour of the dark region in the image will accurately represent the contour of the molecule at a well-defined elevation above the metal surface. As the condensed benzene layer is gradually removed, more of the molecule's contour (lying closer to the tip surface) will be revealed in the image. In real time we observe the morphology of the entire molecule developing before our eyes.

IMAGE DISTORTION

If the clean tip apex is spherical and the condensed benzene layer preserves the symmetry of the tip, the electric field will not be significantly distorted by the presence of the condensed

layer. In this case, image distortion will be determined by local variations in the electric field near the molecule as the molecule is progressively exposed during benzene desorption. Preliminary computer simulations suggest that image distortion is small. Our images of ferritin support this conclusion since they show features which are essentially spherical. However, since the degree of protein denaturing in the ferritin molecule under vacuum conditions is unknown, a quantitative measure of image distortion is impossible to obtain.

It is important to emphasize that our microscope does not require the use of complicated electron lenses to form an image. As a result, image abberation will only occur if the electric field at the tip apex is distorted. Since image contrast is inherently high, the quality of an image will be primarily determined by its resolution.

IMAGE RESOLUTION

The resolution of a blanket-gas image will depend on the size of the blanket-species (since it shadows the molecule's contour) and the temperature of the condensed blanket-gas layer. As the tip temperature is lowered, the resolution of the image will increase because the velocity component of a blanket-gas ion parallel to the tip surface will be reduced. For our purposes, the finite DeBroglie wave-length of the ion can be ignored (i.e. diffraction is negligible). If we assume that a surface species prior to ionization is thermally accommodated to the temperature of the tip, T, its kinetic energy parallel to the tip surface after ionization will be:

$$mV_t^2/2 \sim kT \tag{1}$$

Consider a fixed point on the tip surface. If t is the time that it takes for two adjacent species to travel from the tip to the ion detector, and V_t is their transverse velocity component, then they will have separated by a distance $=2V_t t$ when they reach the detector. The resolution of the image cannot be better than the resulting 'circle of confusion' whose diameter is $2V_t t$. This is equivalent to saying that two species will just be resolved if they are separated by a distance, δ, on the tip surface where:

$$\delta \approx 2V_t t\beta R/D \tag{2}$$

and $D/\beta R$ is the magnification of the image as shown in Fig. 9.

Since an ion will acquire its full kinetic energy very close to the tip surface, its travel time, t, is approximately equal to the time required for it to drift over the tip-to-detector distance, D, with maximum velocity, V_M. That is:

$$t \approx D/V_M = D(m/2neV_0)^{1/2} \tag{3}$$

where m/ne is the mass to charge ratio of the desorbed ion, and V_0 is the potential applied to the tip. Equation (3) assumes that the potential drop across the condensed blanket-gas layer is negligible. If Equations (1)–(3) are combined, the resolution for singly charged blanket gas ions becomes

$$\delta = 2\beta(kTR/KeF)^{1/2} + \delta_0 \tag{4}$$

where the electric field strength $F = V_0/KR$ and the loss in resolution due to the finite diameter to the blanket-gas ion, δ_0, has been included.

For the imaging experiments described in this paper, benzene was chosen as the blanket-gas species, and an electric field was used as the ionization mechanism. Actually, any method which can ionize the condensed blanket-gas layer can be used for imaging purposes. However, since a high field strength is needed to maximize image resolution, field-induced ionization is a convenient approach. It is relatively easy to see that an ideal blanket-gas species would have the following characteristics: (1) a low desorption field, (2) weak binding to neighbouring species within an immobile, multilayer structure, (3) chemical inertness at the field strength required for ionization; and (4) a small ionic diameter. Benzene meets essentially all of these requirements. It field-desorbs at field strengths below 2 V/nm, and gives essentially contrastless images when

desorbed from multilayers deposited on clean tungsten field-emitter tips. It may also be the most chemically inert of the small hydrocarbons in electric fields of ~ 1 V/nm (Röllgen, 1981). However, the diameter of the benzene molecule is large, and will ultimately place a lower limit on the image resolution which can be achieved ($\delta = \delta_0 \sim 0{\cdot}7$ nm).

The low ionization field required of a blanket-gas species effectively precludes the use of all of the common field-ion imaging gases, except possibly hydrogen. The most obvious obstacle to its use may be its apparent mobility on the surface in a high electric field (Jason *et al.*, 1970; Hansen & Siegel, 1979). Figure 10 shows the resolution calculated for desorption of a condensed, immobile benzene layer using Equation (4). For comparison, we also show the resolution which could be achieved if an immobile hydrogen layer could be produced at 5 K. Our ferritin images display a resolution which is consistent with benzene desorption at a tip temperature of 30 K.

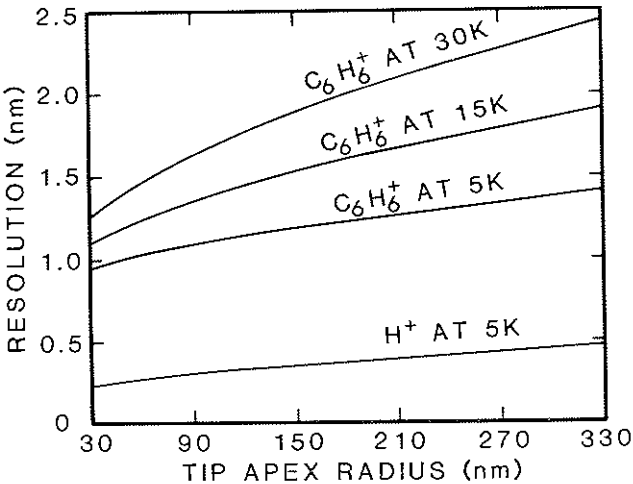

Fig. 10. Theoretical resolution of a point-projection microscope operated with benzene desorbing at 3 V/nm, and hydrogen desorbing at 10 V/nm. The resolution was calculated using Equation (4) in the text, assuming $\beta = 1{\cdot}5$ and $K = 3{\cdot}9$.

APPARATUS

Figure 11 is a schematic drawing of the point-projection microscope which has evolved during this study. In practice, we use a vacuum system which incorporates an airlock to minimize specimen interchange time (Panitz, 1978). Several features of the instrument shown schematically in Fig. 11 should be noted. An infrared, millisecond pulsed laser is used to raise the temperature of the molecule coated tip prior to each imaging event. By using a temperature calibration procedure (Kellogg, 1981) we can assure that the final temperature of the tip will not exceed 300 K. Although a macromolecule should not be disturbed by this temperature, any contaminant species condensed on to the cold tip surface from the ambient vacuum chamber (at 400 nPa) will be thermally desorbed. Without using thermal desorption to 'clean' the tip surface prior to imaging we have found that the image quality will degrade with time, presumably as a result of a gradual but continuous buildup of contaminant species on the apex of the tip.

A retractable capillary tube is used to place a reproducible quantity of benzene on the tip surface (Panitz, 1979a). From our ferritin images we have deduced that the coverage of benzene must be greater than 11 nm. Before the dosing capillary is extended in front of the tip, benzene is allowed to issue from its orifice until an equilibrium pressure (typically 7 μPa as measured in the chamber) is reached. The capillary is then extended for a precise interval of time (usually 3 s) in order to dose the tip. After retracting the capillary, the benzene issuing from the doser orifice is stopped, and the system pumped to 400 nPa before imaging is begun. Since a cryoshield surrounds the tip (except for a small aperture through which the ions pass), benzene

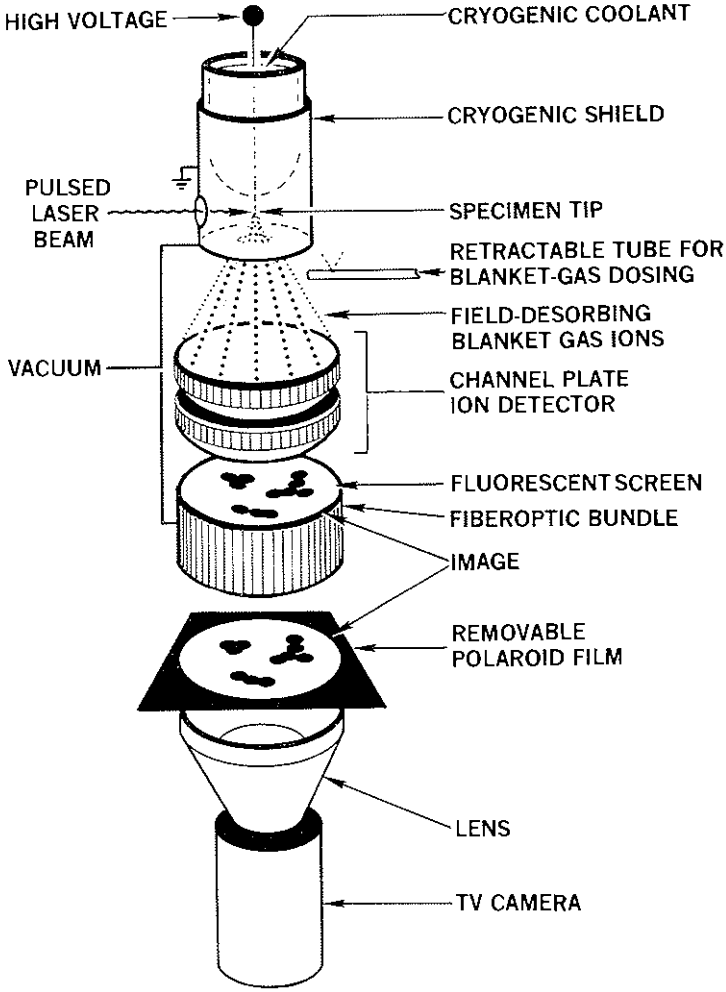

Fig. 11. A schematic drawing of the point-projection microscope used in this investigation. Not shown is a single-ion counting system which records the arrival rate of desorbed benzene ions at the detector as a function of the potential applied to the specimen tip.

deposition on to the tip apex is determined only by the length of time during which the doser remains in its extended position. The background pressure in the system is reduced prior to imaging in order to minimize the chance of space-ionization of benzene above the emitter surface during the imaging process. To obtain images, we typically ramp the voltage applied to the tip at 100 V/s with respect to the grounded cryoshield. All benzene ions desorbed over a 100 V increment of the ramp are photographically or digitally recorded. The process is then repeated so that an image over each successive 100 V increment of the ramp is recorded. Pulsing the tip to successively higher voltages (and remaining at each voltage level for several seconds) yields a completely equivalent series of images.

The benzene ions formed at the surface of the condensed layer travel to a channel plate detector (Panitz, 1978). One novel feature of the detector is the use of a fibre-optic faceplate to transmit the amplified ion image outside of the vacuum system where it can be photographed by direct contact with polaroid film. Alternatively, a TV camera and recording system which incorporates an image digitizer can be used to observe and store the image (Panitz, 1980).

Not shown in Fig. 11 is a single ion counting system, electrically connected to a fluorescent

screen of the detector. As benzene ions strike the detector to produce an amplified electron image on its fluorescent screen, the total number of benzene ions which arrive each second are counted and stored in a multichannel analyser. The analyser is capable of digitizing the incoming ion signal at a rate of 1 MHz. If the channel number of the analyser is advanced in synchronization with the voltage applied to the tip, the desorption rate of benzene can be recorded as a function of tip potential. This feature of the microscopy has proved to be a valuable diagnostic tool during ramp desorption imaging. An example of a field-desorption spectrum will be presented and used to demonstrate the reproducibility of the benzene desorption process.

IMAGING CONSIDERATIONS

If ferritin is deposited on a very thin macroscopic substrate of carbon or Lexan and imaged in the TEM, its outer protein shell (apoferritin) will not be visible without staining. However, its iron-rich core will scatter electrons effectively, and will appear as a dense, opaque spot ~ 6 nm in diameter. Two adjacent ferritin molecules will be seen as two isolated spots, separated by twice the thickness of the apoferritin shell, or ~ 5 nm. Imagine that a Lexan surface is covered with a monolayer of ferritin molecules as judged by ellipsometry or a simple, visual test for protein deposition (Giaever, 1973). We now ask what will the distribution of ferritin be like, when observed in the TEM. We might guess that the ferritin will close pack, thereby satisfying our intuitive feeling of a monolayer coverage. We would only be partially correct.

A recent study of ferritin deposition on thin Lexan films (Feder & Giaever, 1980) demonstrates that although ferritin molecules attempt to cover the entire Lexan surface, large gaps usually remain in the hexagonal close-packed structure which is formed. An example of this phenomena is shown in the TEM micrograph of Fig. 12A. We can simulate the appearance of the entire ferritin molecule by drawing an opaque circle over each imaged core with a diameter equal to the measured distance between two adjacent cores. The result is shown in Fig. 12B. It is instructive to ask what image this distribution of molecules would produce in our point-projection microscope.

We note that the simulated image shown in Fig. 12B corresponds to the contour of individual apoferritin shells at their maximum diameter. In terms of a point-projection image, this would correspond to removing a condensed benzene layer until half of each spherical ferritin molecule is uncovered. We now ask how we can determine this point in an imaging sequence. It is easy to determine when a molecule is just exposed, because a dark region appears in the white benzene background. From that point on, however, the size of the dark region will continue to increase with increasing tip potential until all the benzene is removed from the surface (or until the molecule is field-desorbed). Suppose that the tip potential is increased linearly with time. Since chemisorbed benzene is strongly bound to the surface, the rate of desorption will change as the tip surface is approached. In principle this phenomena can be used to estimate the proper termination point for a desorption ramp.

The maximum diameter of the apoferritin shell should lie approximately half-way between the first contour seen and the last. In order to simulate the image at this point in a desorption sequence, we must include the effect of a finite image resolution. If we assume a tip temperature of ~ 30 K and a tip radius of 160 nm, the resulting resolution is ~ 2 nm, above one-fifth of the diameter of the ferritin molecule. As a result, we would not expect to see the image shown in Fig. 12B, but one similar to that shown in Fig. 12C. In this figure the contours of individual apoferritin shells have been joined and smoothed in accordance with the estimate image resolution.

Before discussing the actual images, a word of caution is in order. The discussion of Fig. 12 was included only as an illustration of what one might expect to see in a point-projection image. We cannot determine the exact distribution of ferritin on the tip apex because we can only view the tip in profile in the TEM over a limited range of axial rotation. Therefore, we only have a sense of the coverage, but not a detailed, two-dimensional map of the position of each ferritin core. Since the deposition and adsorption conditions on our tips are likely to be different than those encountered with the macroscopic surface shown in Fig. 12A, such studies cannot be used

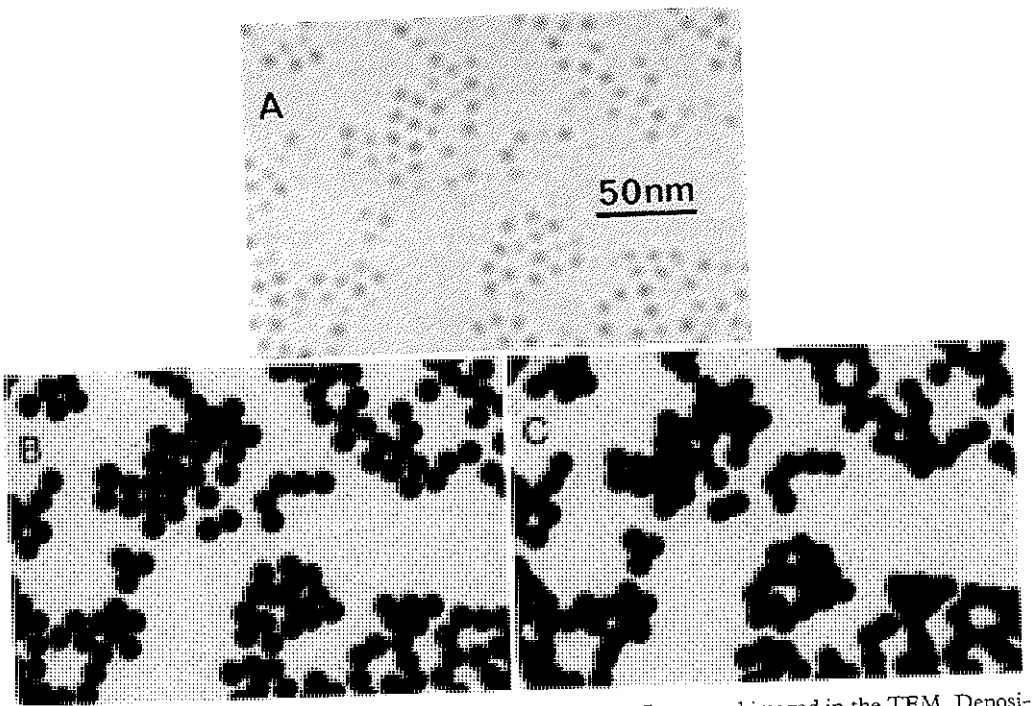

Fig. 12. (A) Ferritin molecules deposited from 0·154 N saline on to Lexan and imaged in the TEM. Deposition parameters were adjusted to produce a monolayer coverage. The protein shell of the molecule (apoferritin) is invisible in this unstained sample, but its iron-rich core can be clearly seen as an opaque spot ~6 nm in diameter. Photograph courtesy of Ivar Giaever, The General Electric Research and Development Center, Schnectady, N.Y. (B) A simulation of the appearance of the entire ferritin molecule in the TEM distribution of (A). The simulation was obtained by drawing an opaque circle (equal in diameter to the apoferritin shell) over each ferritin core. (C) A simulation of a point-projection image of the ferritin distribution at a resolution of ~2 nm.

in a quantitative fashion to interpret our images. However, despite these qualifications, we shall see that our simulated micrograph of Fig. 12C conveys the correct impression of an actual point-projection image.

FERRITIN IMAGING

In order to obtain images which display good contrast and a high signal-to-noise ratio, we have found it desirable to integrate the images obtained from several imaging sequences. Each sequence proceeds as follows: (1) fire the infrared laser at the tip; (2) dose with benzene; (3) (3) ramp the tip bias at 100 V/s from the 0 to V_M; and (4) integrate the benzene ion image which is seen during a 100 V increment of the ramp between voltages V_1 and V_2. The maximum ramp voltage, V_M, is determined in an initial experiment in which the ramp desorption spectrum of benzene is recorded. This will be discussed in the next session.

All video images are recorded in real-time on video tape, while the desired, integrated image between V_1 and V_2 is digitally stored using a real-time digital image processor. Photographic images are produced by direct contact between Polaroid Type 55 film and the fibre-optic faceplate of the CEMA detector. During photographic imaging, the second channel plate of the Chevron pair functions as the shutter of a camera. It is biased 'off', except during the desired integration interval (between V_1 and V_2) when its gain is set to a value dependent upon the amount of benzene desorbed.

Figures 13 and 14 show a sequence of successive images obtained during ramp desorption of benzene from a ferritin coated tip. Figure 13A shows the CEMA background noise recorded

during a 100 V interval of the ramp below the point at which benzene begins to desorb. A micron marker shows the magnification for all of the images in Figs. 13 and 14. The magnification, M, was calculated from the equation $M = D/\beta R$ derived in Fig. 9. D is the measured tip-to-detector distance, and R is the tip radius determined from a TEM micrograph of the tip, shown in Fig. 15. A value of $\beta = 1{\cdot}5$ was chosen in accordance with the value generally accepted for a clean, field-evaporated tip in conventional field-ion microscopy (Müller & Tsong, 1969).

Figure 13B shows benzene desorption early in the ramp. The background is essentially uniform, suggesting that benzene is desorbing from a smooth, condensed layer. As the imaging interval is advanced in increments of 100 V (Figs. 13C–F) the image begins to become more structured. A prominent dark region can be seen in the upper right-hand corner of Fig. 13F. Its appearance early in the imaging sequence as a relatively large area (and its persistence in the remaining images) suggest that it is caused by a cluster of ferritin molecules extending outward from the surface. A careful examination of several TEM micrographs of the tip taken at various axial rotations tends to support this conclusion.

As the ramp proceeds (Figs. 14G–N), structure develops in the image as ferritin clusters are exposed by the receding benzene layer. In Figs. 14K–N a rectangular region of the image

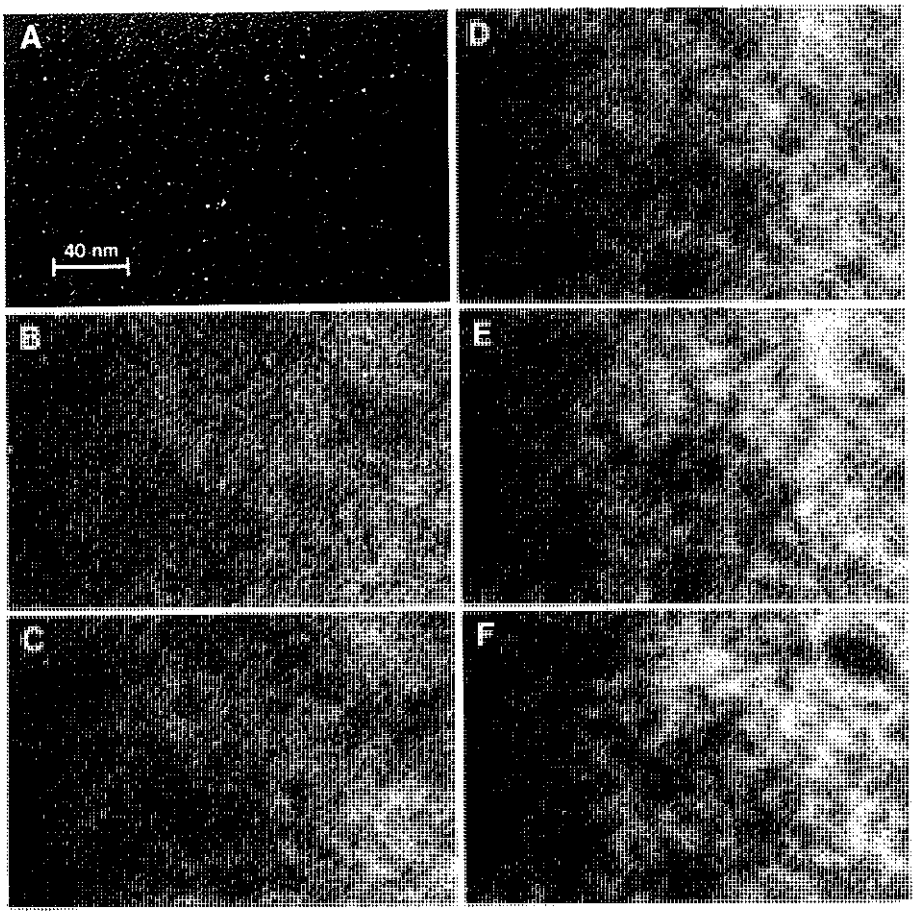

Fig. 13. Benzene desorption from the ferritin coated tip seen in the TEM micrograph of Fig. 15. Each image was obtained by integrating over a 100 V increment of five separate desorption ramps (see text). Figure 13A shows the CEMA dark current before benzene desorption is observed. The voltage increments during imaging (in kV) are as follows: (A) CEMA dark current; 0·55–0·65 (B) 1·7–1·8; (C) 1·8–1·9; (D) 1·9–2·0; (E) 2·0–2·1; (F) 2·1–2·2.

has been outlined and selected for further processing. We wish to construct a three-dimensional image of the ferritin coverage in this area. In order to accomplish this, the rectangular areas were digitized using a Comtal (Vision One/20) image processing system. After selective thresholding to obtain only black and white regions, the image contrast was inverted. The clusters in each figure (which now appear white) were assigned a different grey level between 0 and 255. The images corresponding to ferritin contours furthest from the surface (Fig. 14K) were made the lightest shade of grey; those closest to the surface (Fig. 14N) were made the darkest. Figure

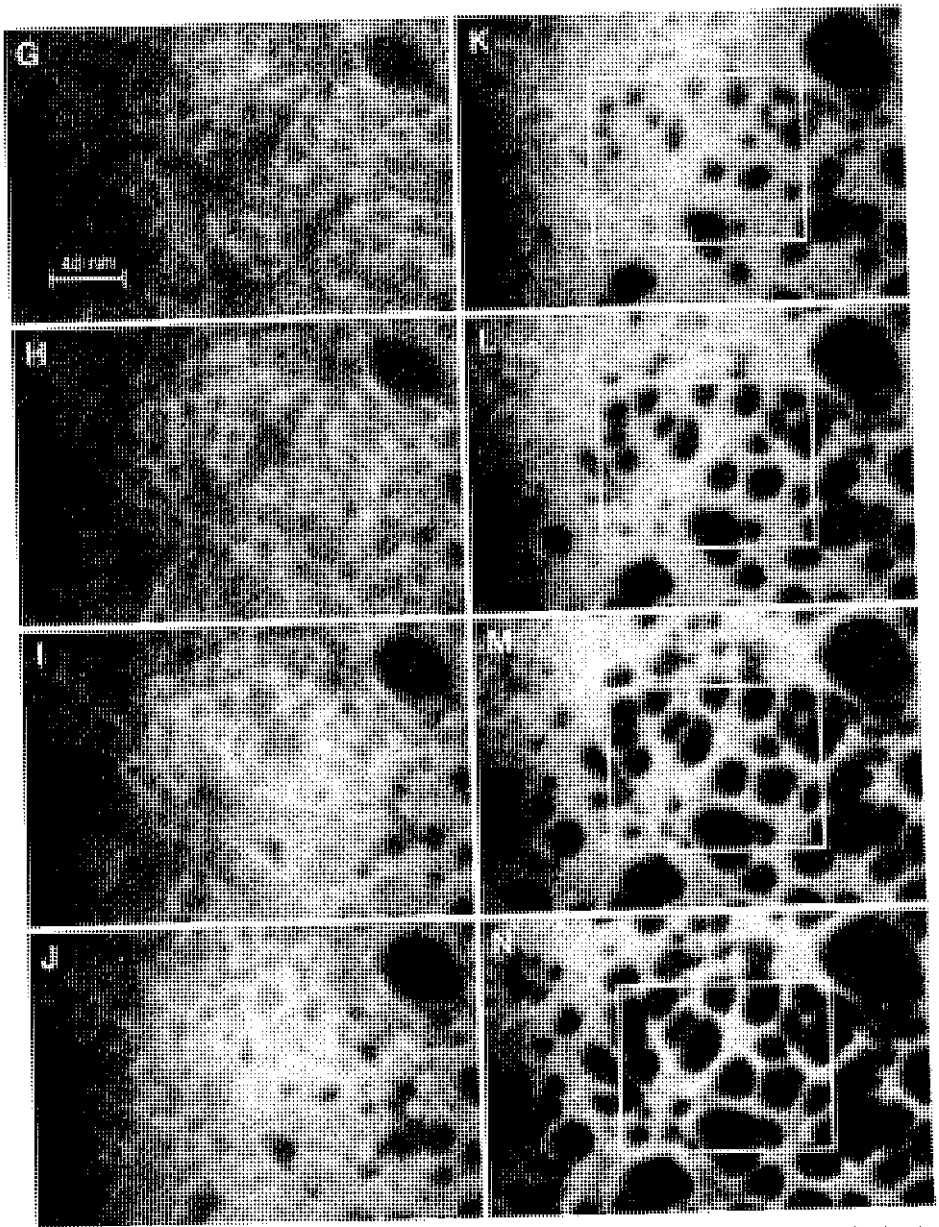

Fig. 14. A continuation of the desorption ramp images of Fig. 13. The voltage increments during imaging (in kV) are as follows: (G) 2·2–2·3; (H) 2·3–2·4; (I) 2·4–2·5; (J) 2·5–2·6; (K) 2·6–2·7; (L) 2·7–2·8; (M) 2·8–2·9; (N) 2·9–3·0.

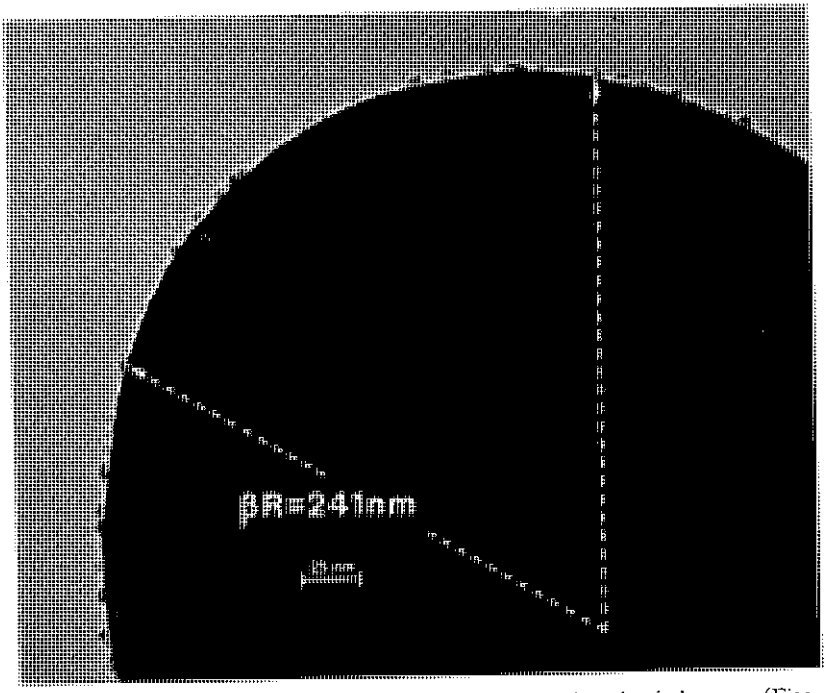

Fig. 15. A TEM micrograph of the ferritin coated tip obtained before imaging in benzene (Figs. 13 and 14). The effective tip radius, βR is shown assuming $\beta = 1{\cdot}5$. The surface area of the tip apex between the dotted lines was available for imaging. Ferritin deposition at 10 μg/ml for 2 min. All dilutions are rinses using 0·154 N saline.

16 shows the image which resulted from linearly super-imposing the four processed images. Clusters and individual molecules of ferritin are seen, with a resolution which appears to be almost as good as the simulated image shown in Fig. 12C. One notes, in particular, the chain of molecules near the centre of Fig. 12C and those appearing at the left-hand edge of the reconstructed image.

It is apparent that a reconstructed image gives a clearer picture of the molecules on the surface than any individual image in the desorption sequence. The distribution of molecular sizes in Fig. 16 is in good agreement with individual apoferritin shells having a diameter of $\sim$11 nm. Since the magnification was obtained by assuming $\beta = 1{\cdot}5$, it appears as though local field enhancement (Rose, 1956) in the vicinity of the ferritin molecule is negligible. It is interesting to speculate about the origin of the irregular shape of some of the features in the reconstructed image. They may reflect denaturing of the unstained apoferritin shell after deposition or after insertion in a high vacuum environment. Since we seem to be able to detect changes in protein morphology after deposition on a metal surface, we may be able to study protein–metal interactions (or at least vacuum denaturing) in more detail than ever before.

The imaging sequence shown in Figs. 13 and 14 is completely reproducible. First, because each image in the sequence was obtained by integrating over the same voltage interval during successive desorption ramps (see Fig. 17). But more importantly because we have reproduced the same images on separate days and even after several months during which time the tip was stored in laboratory ambient. A quick visual examination of the tip in the TEM before and after imaging confirmed that the ferritin distribution had not changed. The speed of the TEM examination is important. We have found that prolonged exposure of the tip apex to the electron beam can cause irreversible changes in the ferritin distribution. In addition, carbon contamination can often be observed (Panitz & Giaever, 1980b) which will eventually obscure the entire distribution.

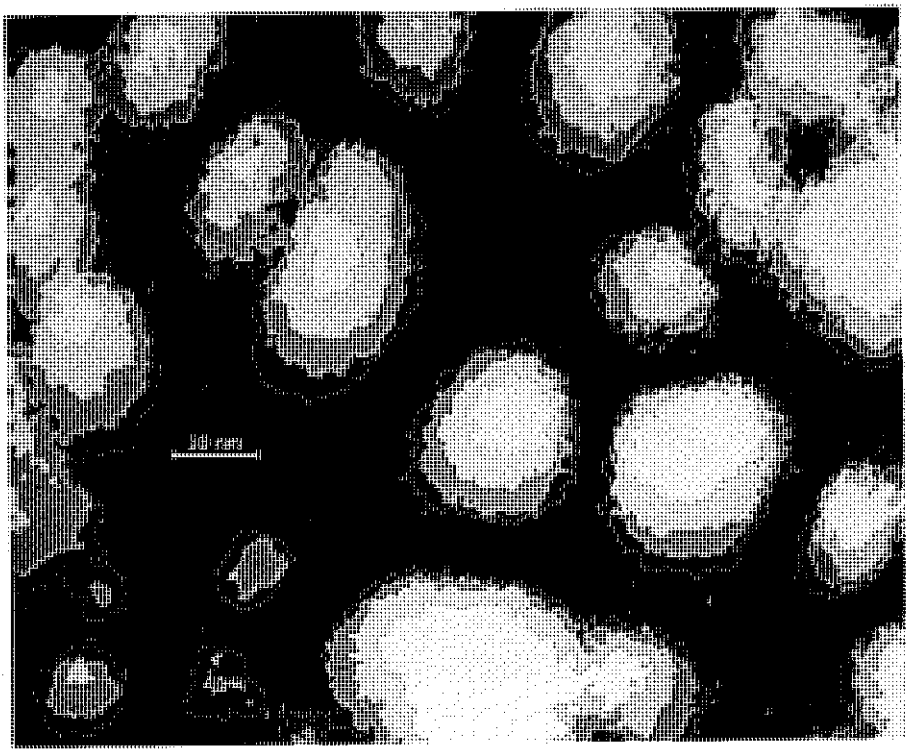

Fig. 16. A three-dimensional reconstruction of ferritin on tungsten corresponding to the area contained within the outlined region of Figs. 14K–N. The lightest regions are furthest from the tungsten surface. The darkest regions are closest to the surface. The protein shell (apoferritin) of the unstained molecule is imaged, in contrast to a TEM micrograph which only shows its iron-rich core.

RAMP-DESORPTION OF BENZENE

Figure 18 shows two typical ramp desorption spectra of benzene from the tungsten tip of Fig. 15. The two spectra (labelled 1 and 2 in the figure) were taken on separate days with the tip stored in vacuum, at room temperature. Since the area under each curve is proportional to the coverage of benzene on the surface, the reproducibility of benzene dosing is confirmed. Furthermore, the identical appearance of the two curves also confirms the reproducibility of the imaging process. In practice, we allow the ramp to advance until the maximum rate of benzene desorption has passed. This defines the maximum tip potential, V_M, which will be applied during imaging. We try to select V_M so that the ramp is terminated before chemisorbed benzene is desorbed from the tungsten surface. The dose of benzene applied to the surface must be critically controlled. By adjusting the dose in order to obtain identical desorption rates, we have successfully imaged different coverages of ferritin on various tips with radii ranging from $\sim$100 nm to $\sim$260 nm.

IMAGING CONSTRAINTS

In order to image a molecule, it must be present on the emitter tip surface within the viewable area of its apex. Our deposition procedure is effective for ferritin, a relatively large, rigid, and stable protein. Other smaller, more flexible molecules may require a modification of the procedure. This may be as simple as changing from physiological saline to a more appropriate dilutent. On the other hand, if surface tension forces during drying (or some other effect) proves to be a problem, an alternate deposition scheme may have to be devised.

The maximum size of a molecule which can be imaged is not unlimited, but is determined by the fixed area of the tip apex accessible by the imaging method. This area is not simply dictated

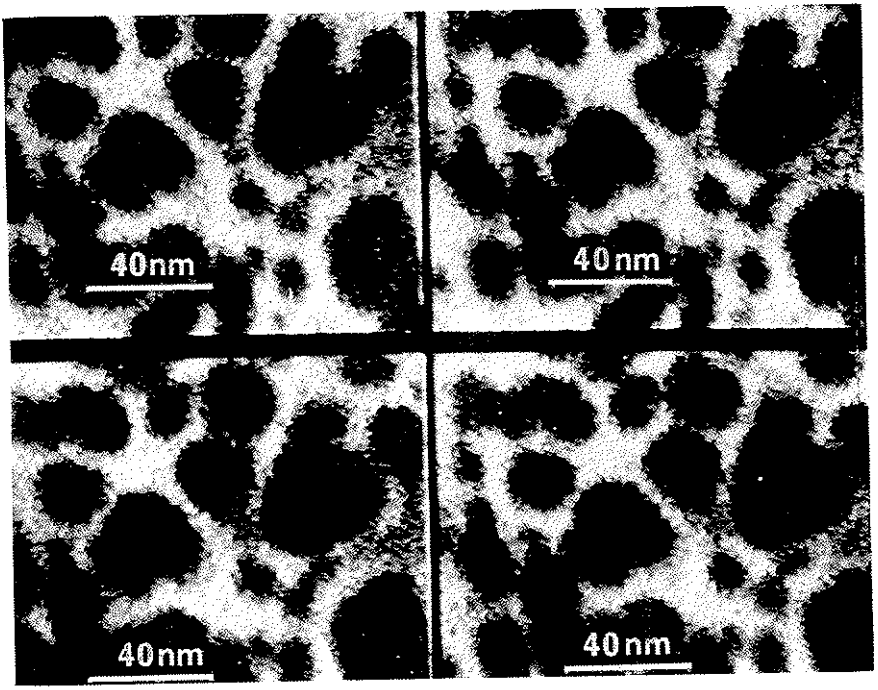

Fig. 17. Four digital images taken over a period of about 1 h. The imaged area roughly corresponds to the area outlined in white in Fig. 14N; however, the orientation and magnification are not identical. Each image was recorded and digitally stored in real time using a TV system and video digitizer (see text).

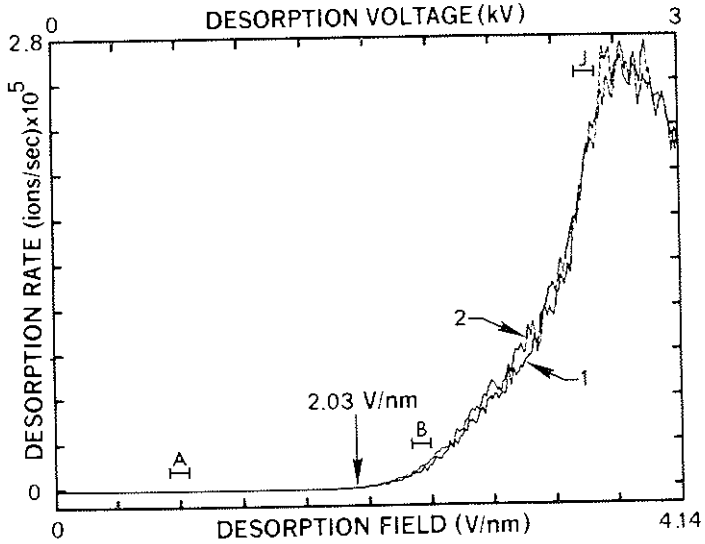

Fig. 18. Ramp desorption spectra of benzene from the ferritin coated tip shown in Fig. 15. The desorption rate of benzene was recorded as a function of desorption voltage. The equivalent desorption field was calculated from a Fowler-Nordheim analysis of electron emission from the clean tip prior to ferritin deposition. A, B and J correspond to 100 V increments in the ramp during which the images of Figs. 13A, 13B and 14J were recorded. Spectrum 1 and 2 were recorded on different days, in order to demonstrate the reproducibility of the benzene closing procedure.

by the geometrical considerations shown in Fig. 9. Because the electric field strength varies with distance from the tip apex (Dyke & Dolan, 1956), the amount of benzene which is desorbed will be a function of position on the surface. This means that at a constant apex field, some molecules will always have more of their morphology exposed than others. In order to eliminate the resulting image ambiguity, we must restrict our field of view to a relatively small angle θ measured from the tip apex.

During a typical desorption ramp to 3 kV (Fig. 18), images are recorded over 100 V intervals. For a negligible change in a given image we have found that the imaging interval must be reproducible to ~ 3 V, or $\sim 0{\cdot}1\%$ of the total ramp range. If the variation in the electric field over the tip surface is similarly limited to $\sim 0{\cdot}1\%$ of the apex field, $\theta \sim \pi/12$ (Dyke & Dolan, 1956; Gomer, 1961). The corresponding imaged area, A, is obtained by assuming that the tip is an isolated sphere in space of radius R. Then, from simple geometry:

$$A = 2\pi R^2(1-\cos\theta) \tag{5}$$

For an actual tip, the effective tip radius is βR (see Fig. 9). If we assume $\beta = 1{\cdot}5$, we obtain:

$$A = 2\pi\beta^2 R^2(1-\cos\theta) \approx (0{\cdot}7R)^2 \tag{6}$$

Since image resolution deteriorates with increasing tip radius (Fig. 10), we cannot choose R to be arbitrarily large. For a typical value of $R = 200$ nm, $A \approx 2\times 10^4$ nm^2. This is equivalent to a maximum (circular) imaged area only 160 nm in diameter. For a CEMA detector 7·5 cm in diameter, the corresponding minimum image magnification is $\sim 2\times 10^5$. If we require at least two molecules to reside within the imaged area, the maximum size of an imaged molecule must be limited to ~ 80 nm.

The minimum size of a molecular feature which can be imaged will be determined by two factors: (1) the resolution of the microscope, and (2) contrast variations inherent in the desorbing benzene layer. The latter will depend on the morphology of the condensed layer, and the anisotropy of the ionization probability. It may be possible to thermally 'anneal' the condensed layer in order to make it more homogeneous. It is not clear how the ionization probability can be made more isotropic.

SUMMARY AND CONCLUSIONS

A point-projection microscopy has been described which has produced images of ferritin molecules deposited on a number of large radius field-emitter tips. The images are non-transient and reproducible, even after repeated exposure of the field-emitter tips to laboratory ambient. Three-dimensional reconstruction of the molecule's morphology from these images suggest that its outer protein shell (apoferritin) is not appreciably distorted. Observable distortion may be caused by the binding properties of ferritin to the tungsten substrate, or denaturing of the molecule in the ultra-high vacuum environment of the microscope. At this time we cannot exclude the possibility of image distortion due to slight asymmetries in the shape of the tip near its apex or local variations in the symmetry of the electric field during imaging. There is no evidence that the imaging process affects the overall structure of the ferritin molecule, provided that a critical electric field strength is not exceeded (Panitz, 1979b).

The diameter of a ferritin molecule can be estimated from a three-dimensional reconstruction of the ferritin covered tip apex. The resulting value of ~ 11 nm is consistent with the diameter of unstained apoferritin which can be deduced from TEM observations of ferritin deposited on to thin carbon films (Iijima, 1977). Since there is no need to envoke a magnification enhancement (Rose, 1956) in order to explain the size of our images, field enhancement in the vicinity of a ferritin molecule appears to be negligible.

Our microscopy provides a means of imaging unstained, isolated, organic molecules deposited on a metallic substrate. However, it is not inherently restricted to organic species. In principle, any object of macromolecular size which can be placed (or fabricated) on the surface of a field emitter tip is a suitable candidate for imaging. Although a dielectric object may produce less field distortion than a metallic object, the latter may still produce a recognizable image. One

must begin to think of the field-emitter tip apex as being sharply pointed, but as a relatively flat substrate upon which a microscopic object is placed for imaging. Over macromolecular distances, even a sharply curved field-emitter can appear infinite in extent.

ACKNOWLEDGMENT

The author wishes to thank the U.S. Department of Energy, Office of Basic Energy Sciences (BES), who generously supported this work under Sandia Contract DE-AC04-76DP00789. Ivar Giaever's desire to 'see' a protein molecule and his unerring belief in experimental simplicity, initiated and guided the early imaging attempts. His enthusiasm and participation in those experiments (and in the protein deposition studies which followed) provided a unique learning experience for the author and are gratefully acknowledged.

Two members of Sandia National Laboratories also deserve special thanks. Gerry Fowler's enthusiasm, cooperation and obvious technical skill made the most difficult part of instrument construction seem easy. Without his daily participation, the present study would have been very difficult to complete. The author also wishes to thank Dennis Ghiglia whose skilful use of a Comtal image processor produced the three-dimensional reconstruction of ferritin shown in this paper.

REFERENCES

Abbott, R.C. (1965) Technique for the deposition of macromolecular samples in field emission and field ion microscopy. *Rev. sci. Instrum.* **36**, 1233.

Becker, J.A. & Brandes, R.G. (1956) A favourable condition for seeing simple molecules in a field emission microscope. *J. appl. Phys.* **27**, 221.

Blodgett, K.B. (1935) Films built by Depositing successive monomolecular layers on a solid surface. *J. Amer. Chem. Soc.* **1935**, 1007.

Dyke, W.P. & Dolan, W.W. (1956) Field emission. In: *Advances in Electronics and Electron Physics* (Ed. by L. Marton), Vol. 8, p. 89 Academic Press, New York.

Feder, J. & Giaever, I. (1980) Adsorption of ferritin. *J. Coll. Interface Sci.* **78**, 144.

Giaever, I. (1973) The antigen–antibody reaction: a visual observation. *J. Immunol.* **110**, 1424.

Gomer, R. (1961) *Field Emission and Field Ionization.* Harvard University Press, Cambridge, Mass.

Graham, W.R., Hutchinson, F. & Reed, D.A. (1973) Field ion microscopy images of DNA and other organic molecules. *J. appl. Phys.* **44**, 5155.

Gurney, T., Jr, Hutchinson, F. & Young, R.D. (1965) Condensation of tungsten on tungsten in atomic detail: observation with the field ion microscope. *J. Chem. Phys.* **42**, 3939.

Hansen, G.R. & Siegel, B.M. (1979) H_2 and rare gases field ion source with high angular current. *J. Vac. Sci. Technol.* **16**, 1875.

Hörl, E. & Strangler, F. (1956) Feldelektronen-Mikroskopische Schirmbilder bei Anwesenheit Organischer dampfe in Versuchsrohr. *Acta Physica Austriaca*, **10**, 1.

Iijima, S. (1977) Thin graphite support films for high resolution electron microscopy. *Micron*, **8**, 41.

Jason, A., Halpern, B., Inghram, M.G. & Gomer, R. (1970) Field ionization from H_2 layers. *J. Chem. Phys.* **52**, 2227.

Kellogg, G.L. (1981) Field emitter temperature calibration in the pulsed laser atom probe. *J. appl. Phys.* **52**, 5320.

Kellogg, G.L. & Panitz, J.A. (1979) The application of high-field surface analytical techniques to the study of plasma-wall interactions in PLT. *Appl. Surf. Sci.* **3**, 13.

Komar, A.P. & Komar, A.A. (1961) Molecules, molecular complexes and atoms as waveguides for electron waves. *Sov. Phys. Tech. Phys.* **6**, 166.

Machlin, E.S. (1971) Low field strength ion microscopy of organic and bio-molecules. Abstract of the 18th International Field Emission Symposium, Eindhoven, The Netherlands, 84 (unpublished).

Machlin, E.S., Freilich, A., Agrawal, D.C., Burton, J.J. & Briant, C.L. (1975) Field ion microscopy of biomolecules. *J. Microsc.* **104**, 127.

Melmed, A.J. (1958) Study of phthalocyanine and some other planar molecules in the field emission microscope. Tech Rep. AFOSR-TN 58-646. ASTIA AD No. 162178.

Melmed, A.J. & Müller, E.W. (1958) Study of molecular patterns in the field emission microscopy. *J. Chem. Phys.* **29**, 1037.

Müller, E.W. (1950a) Sichtbarmachung der Phthalocyanin-Molekel mit dem Feldelektronenmikroskop. *Naturwissenchaften*, **37**, 333.

Müller, E.W. (1950b) Die sichtbarmachungeinzelner Atome under Molekule im Feldelektronenmikroskop. *Z. Naturf.* **5**, 475.

Müller, E.W. (1950c) Smallest molecule ever seen. *Life*, **28** 67 (19 June 1950).

Müller, E.W. (1952) A new microscope. *Sci. Amer.* 186/187, 58 (May 1952).

Müller, E.W. (1953a) Feldemission. *Ergeb. exakt. Naturwissenschaften*, **27**, 290.
Müller, E.W. (1953b) Electron Microscope Society of America (unpublished lecture), see Dyke, W.P. and Dolan, W.W. (1956), p. 139.
Müller, E.W. (1956a) Das Auflosungsvermogen des Feldionenmikroskopes. *Z. Naturf.* **11a**, 88.
Müller, E.W. (1956b) Resolution of the atomic structure of a metal surface by the field ion microscope. *J. appl. Phys.* **27**, 474.
Müller, E.W. & Rendulic, K. (1967) Field ion microscopical imaging of biomolecules. *Science*, **156**, 961.
Müller, E.W. & Tsong, T.T. (1969) *Field Ion Microscopy: Principles and Applications*. Elsevier, New York.
Panitz, J.A. (1975) Single atom mass spectroscopies. Abstracts of the 170th National Meeting of the American Chemical Society, Chicago, Ill., 1975, COLL-009.
Panitz, J.A. (1978) Imaging atom probe mass spectroscopy. *Prog. Surf. Sci.* **8**, 219.
Panitz, J.A. (1979a) Isothermal ramped field-desorption of benzene from tungsten. *J. Vac. Sci. Technol.* **16**, 868.
Panitz, J.A. (1979b) Isothermal Ramped field-desorption of protein layers on Tungsten. Abstracts of the March Meeting of the American Physical Society. *Bull. Amer. Phys. Soc.* **24**, 345.
Panitz, J.A. (1980) Video recording of low intensity CEMA images. *J. Vac. Sci. Technol.* **17**, 757.
Panitz, J.A. (1981) Point-projection imaging of macromolecular contours. Abstracts of the 25th Annual Meeting of the Biophysical Society. *Biophys. J.* **33**, 199a.
Panitz, J.A. & Giaever, I. (1979) Low field imaging of proteins. Abstracts of the 25th International Field-Emission Symposium. *Ultramicroscopy*, **4**, 361.
Panitz, J.A. & Giaever, I. (1980a) Isothermal field desorption imaging of protein macromolecules. Abstracts of the 26th International Field Emission Symposium. *Ultramicroscopy*, **5**, 284.
Panitz, J.A. & Giaever, I. (1980b) Protein deposition on field emitter tips and its removal by UV radiation. *Surf. Sci.* **97**, 25.
Panitz, J.A. & Giaever, I. (1981) Ferritin deposition on field-emitter tips. *Ultramicroscopy*, **6**, 3.
Röllgen, F. (1981) University of Bonn, Bonn, West Germany. Private communication.
Rose, D.J. (1956) On the magnification and resolution of the field electron emission microscope. *J. appl. Phys.* **27**, 215.
Wolf, P. (1954) Die Abbildung molkekularer Objekte mit dem Feldelektronenmikroskop. *Z. angew. Phys.* **6**, 529.